J. Fluid Mech. (1991), *vol.* 231, *pp.* 135–155
Printed in Great Britain

Oscillatory flow and mass transport in a flexible tube

By CAROLYN A. DRAGON AND JAMES B. GROTBERG

Biomedical Engineering Department, Robert R. McCormick School of Engineering and Applied Science, Northwestern University, Evanston, IL 60208, USA *and* Department of Anesthesia, Northwestern University Medical School, Chicago, IL 60611, USA

(Received 17 July 1990 and in revised form 8 January 1991)

The mass transport of a diffusible substance during volume-cycled oscillatory flow in a thin-walled viscoelastic tube is studied. A small-amplitude, long-wavelength travelling wave is generated by the oscillatory pressure gradient. Lubrication theory is employed for slow axial variations to derive regular perturbation solutions to the Navier–Stokes equations. The convection–diffusion equation is solved in a similar manner, assuming uniform steady end concentrations and no wall flux. From the velocity and concentration fields, the time-average rate of axial mass transport is calculated, and its dependence on oscillation frequency, tube stiffness, and stroke amplitude is investigated. The general result is that transport is enhanced less for softer tubes than for stiffer ones and that mass flow rate as a function of frequency reaches a local maximal value. The results are related to gas transport in pulmonary airways during high-frequency ventilation.

1. Introduction

The primary function of the lung is the exchange of oxygen and carbon dioxide. Other substances, such as anaesthetics, aerosols, and toxins, are also delivered and removed from the lungs. Mass transport in the lung depends on convection, diffusion, and their interaction during oscillatory flow. In many clinical situations, a mechanical ventilator is required for breathing. Conventional ventilators mimic the breathing cycle, delivering breaths of 500 ml at a frequency of 15 breaths per minute. As in regular breathing, conventional ventilators rely primarily on convection to transport gases through the upper airways to the respiratory zone, where diffusion becomes the primary transport mechanism. However, in order to obtain tidal volumes comparable with those of the regular breathing cycle, large pressures are required to force the air, which can result in pulmonary barotrauma and impaired cardiac function (Slutsky *et al.* 1980). High-frequency ventilation (HFV) is an alternative type of ventilation under investigation (Bohn *et al.* 1980). In HFV, relatively small tidal volumes of air (35–150 ml) are delivered at high frequencies (5–30 Hz), so that pulmonary barotrauma and cardiac impairment are avoided. Instead of convection alone, HFV relies on the interaction of convection and diffusion to transport gases in the upper airways.

A theoretical model of the lung undergoing HFV would lend insight to the important mechanisms and geometrical features that enhance or inhibit mass transport, leading to the improved design of ventilators and to the development of diagnostic techniques. The simplest model of a pulmonary airway is a straight, rigid tube. Harris & Goren (1967), Chatwin (1975), Watson (1983) and Joshi *et al.* (1983)

studied mass transport during oscillatory flow in such a model. In particular, they studied how the transport rate varies with the Womersley parameter, $\alpha = a(\omega/\nu)^{\frac{1}{2}}$, and the amplitude parameter $A = d/a$, where a is the tube radius, ω the angular frequency of oscillation, ν the kinematic viscosity of the fluid, and d the stroke distance defined by $d = V_T/\pi a^2$, where V_T is the tidal volume. They found that the transport is governed by the interaction of radial diffusion and axial convection and increases monotonically with increasing α for fixed A and Schmidt number, Sc. However, experimental results of HFV (Bohn *et al.* 1980; Rieke, Hook & Meyer 1983; Mitzner, Permutt & Wienmann 1983), suggest the existence of an optimal frequency of oscillation, leading us to the conclusion that a simple, straight, rigid tube is an incomplete model of a pulmonary airway. Indeed, the lungs's airways consist of tapered, curved, branching, flexible-walled tubes of varying length and diameter. Each geometrical and physical feature may enhance or inhibit mass transport at a particular tidal volume or frequency of oscillation. A reasonable approach is to examine each feature individually as a means of understanding the total phenomenon.

The effects of taper on mass transport were studied theoretically by Grotberg (1984) and Godleski & Grotberg (1988) and experimentally by Gaver & Grotberg (1986). Assuming a small taper angle, ϵ, Godleski & Grotberg found solutions for the velocity and concentration fields that were regular perturbation expansions in ϵ. Their results indicate that the rate of axial mass transport in a tapered tube can be greater or less than the straight-tube case, depending on the values of A, α, and ϵ. No local maxima of transport versus α were predicted, however. These papers also investigated the development of bi-directional steady streaming during volume-cycled flow and the steady pressure gradient which evolves. The steady pressure gradient was found to yield higher average pressures at the wider end of the tapered section, and to increase with increasing α. This is consistent with the observation by Simon, Weinmann & Mitzner (1984) of a steady pressure gradient in dog lungs during HFV, with larger pressures near the alveolar zone than at the bronchi. They also observed that the gradient increases with frequency.

Eckman & Grotberg (1988) investigated the effect of tube axial curvature on axial mass transport. In their analysis, δ, the ratio of tube radius to the radius of curvature, was assumed to be small. Solutions to the Navier–Stokes and convection–diffusion equations were posed as regular perturbation expansions in δ. They found that tube curvature increases the rate of axial mass transport for all values of A and α and experiments by Sharp *et al.* (1991) demonstrate this enhancement. Also, when the mass transport rate was plotted against α for certain values of A. Eckmann & Grotberg (1988) showed that a local maximum value of mass transport occurs at some finite value of α. This maximum occurs because of the α-dependent phase relationship between the velocity and concentration fields, the lateral mixing being complicated by secondary flows. As α is increased beyond this local maximum, the transport decreases slightly, and then becomes monotonically increasing with α. Hence the appearance of an optimal frequency for transport during HFV, within a limited range of cycling frequencies, may have contributions from axial curvature effects. Pedley & Kamm (1988) described a model dispersion problem of secondary flow effects and found a resonance behaviour responsible for a local maximum in axial transport.

The effect of wall flexibility on gas exchange efficiency is particularly important, since, unlike curvature or tapering, airway flexibility changes in disease states. In the

lungs, wall flexibility can be interpreted as compliance, which is defined as the pulmonary volume change per unit pressure change. Patients with fibrosis and infant respiratory distress syndrome suffer from decreased compliance. Aging and emphysema tend to increase lung compliance. Understanding the relationship between compliance and gas transport during HFV is essential; a given stroke amplitude and frequency may adequately ventilate one patient, while a completely different set of parameters would be necessary for another. Establishing the dependence of gas exchange efficiency on lung compliance could also enable HFV to be used as a diagnostic tool. Our intent in the present paper is to examine the effect of flexibility on dispersion in a single tube, the fundamental unit comprising the pulmonary airway network, as a means of providing a basis for interpreting overall lung transport behaviour.

Atabek & Lew (1966), amongst many others, studied wave propagation in a viscous fluid contained in an elastic tube. The tube in their model was thin-walled, isotropic, and initially stressed in both the tangential and circumferential directions. They solved the linearized Navier–Stokes equations and examined the resulting waves. In the analysis that follows, we employ Atabek & Lew's model of a flexible tube, with the additional consideration of wall viscosity. First, we solve for the velocity field of oscillatory flow in a flexible tube; next, the concentration field of a diffusible substance is determined; finally, the average axial mass transport rate per cycle is computed. The results are interpreted with respect to pulmonary gas transport.

2. Velocity field: problem formulation

Consider a fluid-filled flexible tube with a right cylindrical coordinate system in which z^* is the axial coordinate, r^* the radial coordinate, and θ the angular coordinate (the asterisks denote dimensional quantities). The tube, which is infinitely long, thin walled, isotropic, and impermeable has the following characteristics: density ρ_0, modulus of elasticity E, damping coefficient g, Poisson's ratio γ, wall thickness h, undisturbed inner radius a, and undisturbed midplane radius R_0^* (note that $a = R_0^* - \frac{1}{2}h$). Both circumferential and longitudinal initial stresses are considered, denoted by $T_{\theta_0}^*$ and $T_{z_0}^*$ respectively. Deformations of the tube take place in both the radial and axial directions, and are denoted by η^* and ξ^* respectively.

The tube is filled with a Newtonian viscous fluid characterized by density ρ and kinematic viscosity ν. We consider only the problem of periodic flow in the tube, so that any transient effects from the starting up of the piston are assumed to have decayed to zero and any end effects at the piston are neglected. Though the tube is considered to be infinitely long, we focus only on a finite portion of the flexible tube, a section of length L. The system is assumed to be isothermal and all body forces within the fluid are neglected. The fluid in the tube is volume-cycled such that a fixed volume of fluid, V_T, passes through the axial position $z^* = 0$ in one half-cycle. We define the angular frequency of oscillation as ω and the stroke length as $d = V_T/\pi a^2$. Because the tube is flexible, the volume-cycling produces travelling wave disturbances in the radial and axial directions in both the wall and the fluid. We define the velocity vector $\boldsymbol{u}^* = (u^*, w^*)$, whose components are in the (r^*, z^*) directions, respectively; because we assume axisymmetric flow, there is no θ-velocity component. Also, let p^* be the pressure difference between the inside and outside of

the tube. All the variables of the problem can be made dimensionless by scaling them as follows:

$$\left.\begin{aligned} r = r^*/a, \quad z = z^*/a, \quad R = R^*/a, \quad \eta = \eta^*/a, \quad \xi = \xi^*/a, \\ u = u^*/\delta U, \quad w = w^*/U, \quad t = \omega t^*, \quad p = p^*/\rho U^2, \end{aligned}\right\} \tag{2.1}$$

where a viscous velocity scale, $U = \nu/a$, has been chosen. For our applications we expect long-wave phenomena, so we employ lubrication theory to define the slowly varying axial coordinate $\zeta = \delta z$ where $\delta \ll 1$ and is inversely proportional to the wavelength of the travelling wave disturbances that propagate down the length of the tube.

Five dimensionless parameters arise from the scalings in (2.1) and appear in the governing equations below. They are defined as follows:

$$A = \frac{d}{a}, \quad \alpha = a\left(\frac{\omega}{\nu}\right)^{\frac{1}{2}}, \quad M = \frac{\rho_0 h}{\rho a}, \quad G = \frac{ga^2}{2\nu}, \quad \kappa = \frac{Ea^2}{\rho_0 \nu^2}. \tag{2.2}$$

Here, A is the amplitude parameter, relating the stroke length to the average inner tube radius, and α is the Womersley parameter (dimensionless frequency) which relates the unsteady acceleration stresses to the viscous stresses of the fluid. The parameters M, G, and κ appear in the stress boundary condition; M is the ratio of wall mass to fluid mass; G is the ratio of wall damping to fluid damping; and κ, the stiffness parameter, relates the radial tube stiffness to the fluid resistance to shear deformations. $\kappa^{\frac{1}{2}}$ may also be interpreted as a wave speed ratio where $(E/\rho_0)^{\frac{1}{2}}$ is a characteristic elastic wave speed and ν/a is a characteristic fluid shear propagation speed.

The behaviour of the fluid is governed by the Navier–Stokes equations in cylindrical coordinates. In dimensionless form they are

$$\alpha^2 \frac{\partial u}{\partial t} + \delta u \frac{\partial u}{\partial r} + \delta w \frac{\partial u}{\partial \zeta} = -\frac{1}{\delta}\frac{\partial p}{\partial r} + \frac{1}{r}\frac{\partial u}{\partial r} + \frac{\partial^2 u}{\partial r^2} + \delta^2 \frac{\partial^2 u}{\partial \zeta^2} - \frac{u}{r^2}, \tag{2.3a}$$

$$\alpha^2 \frac{\partial w}{\partial t} + \delta u \frac{\partial w}{\partial r} + \delta w \frac{\partial w}{\partial \zeta} = -\delta \frac{\partial p}{\partial \zeta} + \frac{1}{r}\frac{\partial w}{\partial r} + \frac{\partial^2 w}{\partial r^2} + \delta^2 \frac{\partial^2 w}{\partial \zeta^2}, \tag{2.3b}$$

and the conservation of mass for an incompressible fluid is given by

$$\frac{\partial u}{\partial r} + \frac{u}{r} + \frac{\partial w}{\partial \zeta} = 0. \tag{2.4}$$

The no-slip boundary condition is

$$\delta u = \alpha^2 \frac{\partial \eta}{\partial t} \quad \text{at} \quad r = R(z,t) - \frac{h}{2a}, \tag{2.5a}$$

$$w = \alpha^2 \frac{\partial \xi}{\partial t} \quad \text{at} \quad r = R(z,t) - \frac{h}{2a}. \tag{2.5b}$$

We also impose a balance of the internal, inertial, and surface forces on the wall. A stress boundary condition is derived by Atabek & Lew (1966) for a thin-walled, axisymmetric elastic tube. Adding a wall damping force to their condition gives the

stress boundary condition for a viscoelastic tube. The radial component has the dimensionless form

$$\frac{1}{R\Gamma^{\frac{1}{2}}}\left[T_{\theta_0}+\frac{M\kappa}{1-\gamma^2}\left(\frac{\eta}{R}+\delta\gamma\frac{\partial\xi}{\partial\zeta}\right)\right]-\delta^2\frac{1}{\Gamma^{\frac{3}{2}}}\frac{\partial^2 R}{\partial\zeta^2}$$
$$\times\left[T_{t_0}+\frac{M\kappa}{1-\gamma^2}\left(\delta\frac{\partial\xi}{\partial\zeta}+\gamma\frac{\eta}{R}\right)\right]-\frac{1}{\Gamma}M\alpha^4\left[\delta\frac{\partial R}{\partial\zeta}\left[\frac{\partial^2\xi}{\partial t^2}+\frac{2G}{\alpha^2}\frac{\partial\xi}{\partial t}\right]-\frac{\partial^2\eta}{\partial t^2}-\frac{2G}{\alpha^2}\frac{\partial\eta}{\partial t}\right]$$
$$-\left\{p+\frac{2\delta}{\Gamma}\left[\frac{\partial R}{\partial\zeta}\left(\frac{\partial w}{\partial r}+\delta^2\frac{\partial u}{\partial\zeta}\right)-\frac{\partial u}{\partial r}-\delta^2\left(\frac{\partial R}{\partial\zeta}\right)^2\frac{\partial w}{\partial\zeta}\right]\right\}=0 \quad \text{at} \quad r=R-h/2a, \tag{2.6a}$$

and the axial component is given by

$$\delta\frac{\partial R}{\partial\zeta}\left[T_{t_0}-T_{\theta_0}+\frac{M\kappa}{1-\gamma^2}\left(\delta(1-\gamma)\frac{\partial\xi}{\partial\zeta}-\frac{\eta}{R}\right)\right]$$
$$+\delta R\frac{M\kappa}{1-\gamma^2}\left[\delta\frac{\partial^2\xi}{\partial\zeta^2}+\frac{\gamma}{R}\frac{\partial\eta}{\partial\zeta}\right]-M\alpha^4 R\left[\delta\frac{\partial R}{\partial\zeta}\frac{\partial^2\eta}{\partial t^2}+\frac{\partial^2\xi}{\partial t^2}+\frac{2G}{\alpha^2}\frac{\partial\xi}{\partial t}\right]$$
$$+\frac{R}{\Gamma^{\frac{1}{2}}}\left\{\delta^2\frac{\partial R}{\partial\zeta}\left(\frac{\partial w}{\partial\zeta}-\frac{\partial u}{\partial r}\right)+\left[\delta^2\left(\frac{\partial R}{\partial\zeta}\right)^2-1\right]\left[\frac{\partial w}{\partial r}+\delta^2\frac{\partial u}{\partial\zeta}\right]\right\}=0 \quad \text{at} \quad r=R-h/2a. \tag{2.6b}$$

The quantity Γ is defined as $\Gamma=1+\delta^2(\partial R/\partial\zeta)^2$.

At this point in the analysis we introduce the volume-cycling condition, which ensures a fixed leading-order tidal volume at a given axial position. Considering again the dimensional coordinate system, at a fixed axial position, say $z^*=0$, and in the limit $\delta\to 0$, we constrain the axial velocity to a fixed stroke volume, V_T, defined as

$$V_T=\int_{t_0^*}^{t_1^*}\int_0^{2\pi}\int_0^a w_0^*(r^*,0,t^*)\,r^*\,\mathrm{d}r^*\,\mathrm{d}\theta\,\mathrm{d}t^*, \tag{2.7}$$

where the time interval t_0^* to t_1^* is the time it takes for a full unidirectional stroke of the piston. Scaling the above equation, recalling the definition $V_T=d\pi a^2$, and integrating once with the appropriate values for t_0 and t_1 we obtain the dimensionless volume flow rate condition

$$\int_0^1 w_0(r,0,t)\,r\,\mathrm{d}r=\tfrac{1}{8}A\alpha^2\,\mathrm{e}^{\mathrm{i}t}+\text{c.c.} \tag{2.8}$$

where c.c. denotes the complex conjugate.

3. Velocity field: method of solution

To determine a solution for the velocity field and pressure, we use an asymptotic expansion of each dependent variable in powers of δ, the long-wavelength parameter. These expansions have the form

$$u(r,\zeta,t)=u_0(r,\zeta,t)+\delta u_1(r,\zeta,t)+O(\delta^2), \tag{3.1a}$$
$$w(r,\zeta,t)=w_0(r,\zeta,t)+\delta w_1(r,\zeta,t)+O(\delta^2), \tag{3.1b}$$
$$p(r,\zeta,t)=\frac{1}{\delta}[p_0(r,\zeta,t)+\delta p_1(r,\zeta,t)+O(\delta^2)]. \tag{3.1c}$$

The axial pressure gradient is assumed to be an order larger than the fluid velocities

in order to provide a driving force for the fluid to balance the local acceleration and viscous terms in (2.3b).

For our applications we expect small-amplitude disturbances of the wall, so it is appropriate at this point to introduce another small parameter, ϵ, which represents the order of magnitude of the radial wall displacement. Therefore, we propose asymptotic expansions of the wall displacements of the form

$$\eta(\zeta,t) = \epsilon\eta_1(\zeta,t)+\epsilon^2\eta_2(\zeta,t)+O(\epsilon^3), \tag{3.2a}$$

$$\xi(\zeta,t) = \epsilon\xi_1(\zeta,t)+\epsilon^2\xi_2(\zeta,t)+O(\epsilon^3), \tag{3.2b}$$

and assume that $\epsilon = b\delta$, where b is $O(1)$. Indeed, we set $b = 1$ for the remaining analysis.

The assumption of small-amplitude wall displacements enables us to relate the midplane radius to the radial wall displacement

$$R(\zeta,t) = R_0+\eta(\zeta,t). \tag{3.3}$$

It can be shown that relation (3.3) is true to $O(\delta^2)$. As a result, the free boundary of the fluid, previously described as $r = R-h/2a$, may be replaced by $r = 1+\eta(\zeta,t)$. In the no-slip and stress boundary conditions above (equations (2.5–2.6)), we are required to evaluate the field variables (w,u,p) of the form $f = f(r,\zeta,t)$ at the unknown boundary, $r = 1+\eta$. Using Taylor's theorem, together with the asymptotic expansion in δ, the boundary conditions can be expanded about the known position $r = 1$, where each field variable at the boundary takes the form

$$f(1+\eta,\zeta,t) = f_0(1,\zeta,t)+\delta\left[f_1(1,\zeta,t)+\eta_1(\zeta,t)\frac{\partial f_0(1,\zeta,t)}{\partial r}\right]+O(\delta^2). \tag{3.4}$$

Finally, we wish to preserve the wall inertia and initial stresses in the stress boundary conditions in the limit $\delta\to 0$. To do this, we define

$$\hat{M} = \delta^2 M, \quad \hat{T}_{t_0} = \delta^2 T_{t_0}, \quad \hat{T}_{\theta_0} = \delta T_{\theta_0}. \tag{3.5}$$

Inserting the above expansions for u, w, p, η, and ξ into the governing equations and equating to zero the coefficient of each power of δ gives a set of linear partial differential equations at successive orders of δ. The first two orders of this substitution, $O(1/\delta^2)$ and $O(1/\delta)$ in (2.3a), dictate that $\partial p_0/\partial r = 0$ and $\partial p_1/\partial r = 0$. At $O(1)$ the uncoupled set of partial differential equations have travelling wave solutions of the form

$$w_0 = W_0(r)\,\mathrm{e}^{-\mathrm{i}(k\zeta-t)}+\text{c.c.} = \frac{A\alpha^2}{4}\frac{J_0(\sigma)}{J_2(\sigma)}\left[\frac{J_0(\sigma r)}{J_0(\sigma)}-1\right]\mathrm{e}^{-\mathrm{i}(k\zeta-t)}+\text{c.c.}, \tag{3.6a}$$

$$u_0 = U_0(r)\,\mathrm{e}^{-\mathrm{i}(k\zeta-t)}+\text{c.c.} = \frac{\mathrm{i}A\alpha^2}{4}k_0\frac{J_0(\sigma)}{J_2(\sigma)}\left[\frac{J_1(\sigma r)}{\sigma J_0(\sigma)}-\frac{r}{2}\right]e^{-i(k\zeta-t)}+\text{c.c.}, \tag{3.6b}$$

$$p_0 = \frac{\hat{T}_{\theta_0}}{R_0} = P_0\,\mathrm{e}^{-\mathrm{i}(k\zeta-t)}+\text{c.c.} = -\frac{1}{4k_0}A\alpha^4\frac{J_0(\sigma)}{J_2(\sigma)}\mathrm{e}^{-\mathrm{i}(k\zeta-t)}+\text{c.c.}, \tag{3.6c}$$

$$\eta_1 = H_1\,\mathrm{e}^{-\mathrm{i}(k\zeta-t)}+\text{c.c.} = \tfrac{1}{8}Ak_0\,\mathrm{e}^{-\mathrm{i}(k\zeta-t)}+\text{c.c.}, \tag{3.6d}$$

$$\xi_1 = 0. \tag{3.6e}$$

In the above expressions J_n is the Bessel function of the first kind of order n, $\sigma = \alpha\mathrm{i}^{\frac{3}{2}}$ and we introduce k, the wavenumber, which has the form

$$k = k_0+\delta k_1+O(\delta^2). \tag{3.7}$$

The solution to the governing equations also yields an expression for the leading-order wavenumber k_0 of the form

$$k_0 = \pm\left[\frac{2J_0(\sigma)}{J_2(\sigma)}\frac{R_0^2\alpha^4}{\hat{M}[R_0^2\alpha^4 - iR_0^2(2G)\alpha^2 - \kappa/(1-\gamma^2)]}\right]^{\frac{1}{2}}. \tag{3.8}$$

We choose the positive travelling wave, positive root, for our analysis and will denote as k_{0R} and k_{0I} the real and imaginary parts of k_0, respectively.

The $O(\delta)$ solutions for w_1 and p_1 consist of a sum of periodic, doubly periodic and steady terms:

$$w_1 = W_1^{(0)}(r)\,e^{2k_I\zeta} + W_1^{(1)}(r)\,e^{-i(k\zeta-t)} + W_1^{(2)}(r)\,e^{-2i(k\zeta-t)} + \text{c.c.}, \tag{3.9a}$$

$$p_1 = P_1^{(0)}\,e^{2k_I\zeta} + P_1^{(2)}\,e^{-2i(k\zeta-t)} + \text{c.c.} \tag{3.9b}$$

As a result, we expect steady streaming in both the axial and radial directions. These steady velocities are most prominent near $\zeta = 0$ and decay along the length of the tube. Because of the steady streaming and steady pressure gradient, there is also a time-independent radial deformation of the tube superimposed on the travelling wave deformation. Looking ahead to the mass transport rate calculation, we see that the relevant information for our analysis at this order is the steady axial velocity. Separating variables in the $O(\delta)$ fluid equations and solving for the steady axial velocity profile gives

$$W_1^{(0)}(r) = \tfrac{1}{2}k_{0I}P_1^{(0)}r^2 + \psi(r) + l_1, \tag{3.10}$$

where the quantity $\psi(r)$ is defined as

$$\psi(r) = \int_0^r \frac{1}{q}\int_0^q \left[\bar{U}_0\frac{dW_0}{ds} - ik_0\,\bar{W}_0\,W_0\right] s\,ds\,dq \tag{3.11}$$

in which the overbars indicate complex conjugate. $P_1^{(0)}$, the steady pressure amplitude, and l_1, the constant of integration, are determined by the boundary conditions and can be expressed as

$$P_1^{(0)} = \frac{-4}{k_{0I}}\left[b\bar{H}_1\left(\frac{dW_0}{dr}(1) + \frac{1}{k_{0I}}\frac{dU_0}{dr}(1)\right) + \psi(1) - 2\int_0^r \psi(r)\,r\,dr\right], \tag{3.12}$$

$$l_1 = b\bar{H}_1\left(\frac{dW_0}{dr}(1) + \frac{2}{k_{0I}}\frac{dU_0}{dr}(1)\right) + \psi(1) - 4\int_0^r \psi(r)\,r\,dr. \tag{3.13}$$

4. Velocity field: results

The wavenumber, velocity field, and wall displacements depend on the dimensionless parameters discussed earlier. We are most interested in determining the effect of flexibility, κ, on the system over a range of frequencies, α. The following results were obtained for fixed mass parameter $M = 49$, and damping parameter $G = 13.4$. These values were computed using approximate values of ρ, ρ_0, h, a, ν, D_m (the molecular diffusivity) and g for air in the trachea; their numerical values and the basis on which they were chosen are discussed in the Appendix. Unless otherwise specified, the amplitude parameter is fixed at $A = 5$. Also, the initial wall stress T_{θ_0} is assigned a value of 0.01, and we choose $\delta = 0.1$ and $\epsilon = \delta$ so that $b = 1$. We consider values of κ between 10^3 (representing a very flexible tube) and 10^8 (representing a nearly rigid tube), and values of dimensionless frequency $1 \leqslant \alpha \leqslant 12$. For the fixed A, M, and G discussed above, these parameter ranges correspond to moduli of elasticity between 28 and 2.8×10^6 and cycling frequencies between 0.03 and 4.2 Hz.

We are interested in the response of the flexible-walled tube, particularly in the

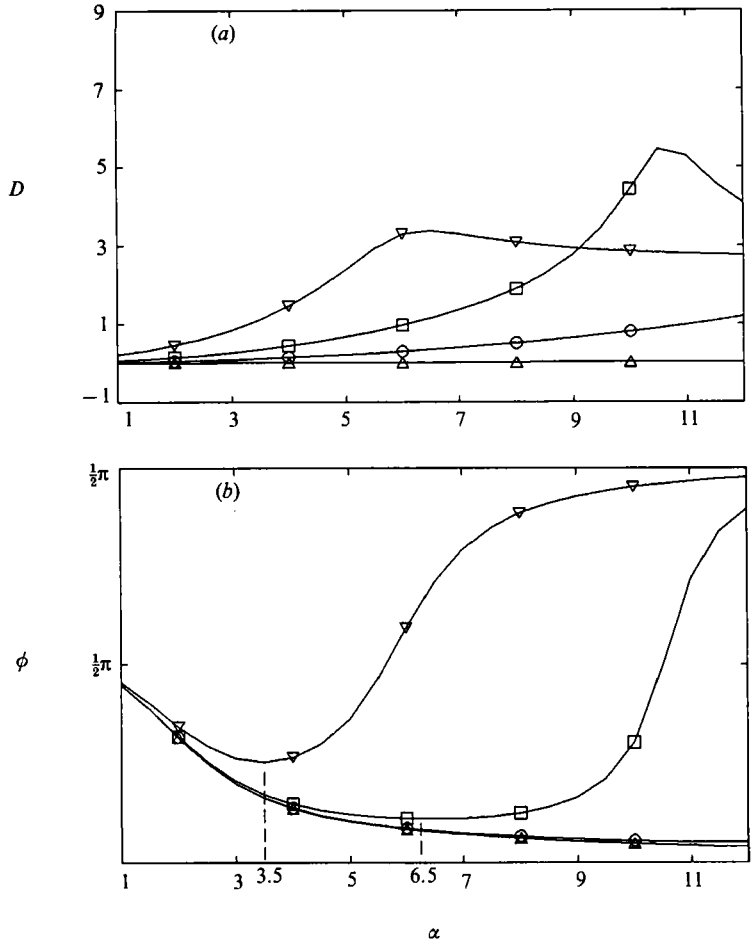

FIGURE 1. Radial wall position at $\zeta = 0$, $\eta = D\cos(t-\phi)$, as a function of α, and for ∇, $\kappa = 10^3$; $\square$, $\kappa = 10^4$; $\bigcirc$, $\kappa = 10^5$; $\triangle$, $\kappa = 10^8$. (*a*) D, the peak radial wall displacement amplitude; (*b*) ϕ, the phase angle.

radial direction, to the motion of the fluid. To leading order, the radial wall motion η_1, evaluated at $\zeta = 0$, may be expressed as

$$\eta_1(\zeta = 0) = D\cos(t-\phi), \tag{4.1}$$

where D is the displacement amplitude and ϕ the phase difference between the forcing of the fluid (the flow rate $q = Q\cos(t)$) and the response of the wall. This phase lag is determined by the damping in the system and by the relationship between the natural and forcing frequencies. The amplitude D is also affected by the damping, natural frequency, and forcing frequency, as well as the forcing amplitude.

Figure 1 (*a*) illustrates how D, the radial wall displacement amplitude, varies with α, the dimensionless frequency, for $\kappa = 10^3$, 10^4, 10^5, and 10^8. For the case $\kappa = 10^8$, the amplitude is negligible for most α in the parameter range, which is in agreement with the earlier assumption that $\kappa = 10^8$ represents a rigid tube. In the cases $\kappa = 10^3$ and $\kappa = 10^4$, D reaches a local maximum. The case $\kappa = 10^5$ neither peaks nor levels off in this parameter range. Note that after the $\kappa = 10^4$ and $\kappa = 10^3$ curves intersect, the stiffer tube has a larger displacement amplitude.

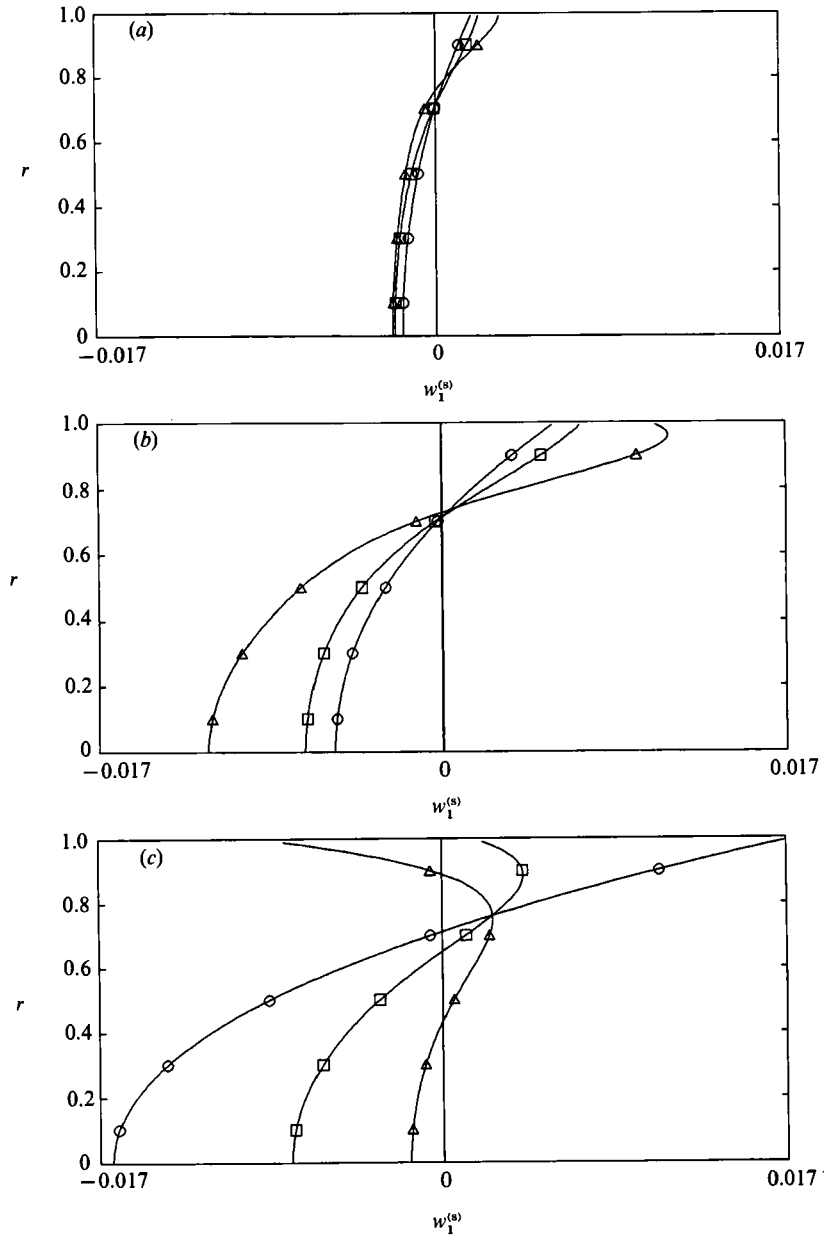

FIGURE 2. Steady axial velocity profile at $\zeta = 0$ as a function of r, for ○, $\alpha = 2$; □, $\alpha = 6$; △, $\alpha = 10$: (*a*) $\kappa = 10^5$; (*b*) $\kappa = 10^4$; (*c*) $\kappa = 10^3$.

The relationship between ϕ, the phase angle, and α is illustrated in figure 1 (*b*) for the same cases as in figure 1 (*a*). Recall that ϕ represents the phase difference between the forcing of the fluid and the response of the wall. For all values of κ shown, ϕ has approximately the same value for small α. In the cases $\kappa = 10^5$ and $\kappa = 10^8$, the phase lag decreases asymptotically to zero, in this parameter range, while the softer tubes, $\kappa = 10^3$ and $\kappa = 10^4$ exhibit local minima which are indicated. Both the $\kappa = 10^4$ and $\kappa = 10^3$ curves approach $\phi = \frac{1}{2}\pi$ as α increases, suggesting that for these cases, high frequencies result in wall responses that are a quarter of a cycle out of phase with the

flow. Note that the minimum values of the (ϕ,α)-curves shift to the left as κ decreases, suggesting that the response of more flexible tubes are most in phase with the driving force at lower frequencies.

Turning our attention to the motion of the fluid, we examine the axial steady streaming found at $O(\delta)$ which results from the nonlinear wave mechanics. Figure 2(*a–c*) illustrates the steady velocity field, $w_1^{(s)}$, at the fixed axial position $\zeta = 0$ for $\alpha = 2$, 6, and 10, and for the cases $\kappa = 10^5$, 10^4, and 10^3. The $\kappa = 10^8$ case is not shown since it models an essentially rigid tube in which the steady streaming is negligible. Note that in each part of the figure, the velocity at $r = 1$ is non-zero because the no-slip boundary condition at this order requires zero axial velocity at the boundary $r = 1+\eta$. For $\kappa = 10^4$ and $\kappa = 10^5$, we generally have positive streaming near the wall and negative streaming in the core. It is interesting to note that for $\alpha = 2$ and $\alpha = 6$, the amplitude of the steady streaming increases as the stiffness, κ, decreases. However, at higher frequencies, $\alpha = 10$, the steady streaming velocity increases in amplitude only between $\kappa = 10^5$ and $\kappa = 10^4$, and then decreases, in the core, as κ goes from 10^4 to 10^3 while developing flow reversal near the wall boundary. It is interesting to compare these results to those of Grotberg (1984), Gaver & Grotberg (1986), and Godleski & Grotberg (1988) in which steady streaming was examined for oscillatory flow in tapered tubes and channels. They found that for $\alpha \leqslant 6$, approximately, steady streaming was positive (towards the wider end of the tapered tube) in the core and negative near the wall, exactly the opposite of the results discussed above for a flexible tube where we consider $\zeta = 0$ to coincide with the proximal tube end. However, at higher frequencies of oscillation, they found steady streaming velocities similar to those pictured in the $\alpha = 10$ case of figure 2(*c*). These comparisons suggest that the effects of taper and flexibility on steady streaming may compete at low frequencies and reinforce each other at high frequencies. Calculations of the $O(\delta)$ steady axial pressure gradient indicate that $\partial p_1^{(s)}/\partial\zeta > 0$ over a wide range of parameters. This is similar to the steady pressure gradient in a rigid tapered tube (Godleski & Grotberg 1988), in which the steady pressure at the wider end is greater than at the narrow end. It is noteworthy that these two results are consistent with the observations and pressure measurements during high-frequency ventilation by Simon *et al.* (1984), discussed in the introduction.

5. Concentration field: problem formulation

Using the results for the velocity field, the transport of a dissolved species within the tube can be determined from the convection–diffusion equation, which governs the transport of a soluble substance with molecular diffusivity D_m. In dimensionless circular cylindrical coordinates, assuming axisymmetric transport, the equation takes the form

$$Sc\left[\alpha^2\frac{\partial c}{\partial t}+u\frac{\partial c}{\partial r}+\delta w\frac{\partial c}{\partial \zeta}\right]=\frac{\partial^2 c}{\partial r^2}+\frac{1}{r}\frac{\partial c}{\partial r}+\delta^2\frac{\partial^2 c}{\partial \zeta^2}, \tag{5.1}$$

where c^* has been scaled on $\hat{c}$, the steady concentration at the axial position $z^* = 0$. The new dimensionless parameter that appears above is the Schmidt number, $Sc = \nu/D_m$, which can be thought of as the ratio of the rate of fluid vorticity diffusion to contaminant diffusion. By retaining the lubrication scale, $\zeta = \delta z$, in the above equation, the concentration field is assumed to vary slowly in the axial direction.

Because the tube wall is impermeable, a no-flux condition is imposed at the wall so that

$$\boldsymbol{n}\cdot\nabla c = 0 \quad \text{at} \quad r = 1+\eta, \tag{5.2}$$

where the unit normal $\boldsymbol{n}$ is defined as

$$\boldsymbol{n} = \nabla F/|\nabla F|, \tag{5.3}$$

and $F(r,z,t) = r - R(\zeta,t) = 0$. We also prescribe the time-independent concentration at two fixed axial reference points in the tube, say at $\zeta = 0$ and $\zeta = l = \delta L/a$, so that

$$c^{(s)}(r,0) = 1, \quad c^{(s)}(r,l) = 0, \tag{5.4}$$

where, as before, the superscript (s) indicates the steady component. The above condition allows the concentration to vary at the specified axial positions over the course of a periodic cycle, but requires that the steady component of the concentration at those points be constant.

6. Concentration field: method of solution

The appearance of the small parameter δ in the convection–diffusion equation suggests a solution for the concentration field in the form of a regular perturbation expansion:

$$c(r,\zeta,t) = c_0(r,\zeta,t) + \delta c_1(r,\zeta,t) + O(\delta^2). \tag{6.1}$$

Substituting (3.1*a*, *b*) and (6.1) into the convection–diffusion equation gives a linear boundary-value problem at each order of δ. Taylor's theorem is used to expand the no-flux condition about the radial position $r = 1$. The resulting leading-order equation and boundary conditions dictate that c_0 is independent of time and radial position, so that $c_0 = c_0(\zeta)$, but the functional dependence of c_0 on ζ is still unknown.

At $O(\delta)$ the convection–diffusion equation is a balance of the unsteady term with radial diffusion and axial convection. It has travelling wave solutions of the form

$$c_1 = \frac{\mathrm{d}c_0}{\mathrm{d}\zeta}[C_1(r)\,\mathrm{e}^{-\mathrm{i}(k\zeta - t)} + \text{c.c.}], \tag{6.2}$$

where $\mathrm{d}c_0/\mathrm{d}\zeta$ is yet undetermined and $C_1(r)$ is solved by using the method of variation of parameters and can be expressed as

$$C_1 = \beta_1 J_0(\sigma Sc^{\frac{1}{2}} r) + Z_1(r)\, J_0(\sigma Sc^{\frac{1}{2}} r) + Z_2(r)\, Y_0(\sigma Sc^{\frac{1}{2}} r), \tag{6.3}$$

where

$$Z_1(r) = -\tfrac{1}{2}\pi Sc \int_0^r W_0(s)\, Y_0(\sigma Sc^{\frac{1}{2}} s)\, s\,\mathrm{d}s, \tag{6.4a}$$

$$Z_2(r) = \tfrac{1}{2}\pi Sc \int_0^r W_0(s)\, J_0(\sigma Sc^{\frac{1}{2}} s)\, s\,\mathrm{d}s, \tag{6.4b}$$

and β_1 is determined by the no-flux condition. Y_0 is the zeroth-order Bessel function of the second kind, and W_0 is the radial dependence of the leading-order axial fluid velocity given in (3.10).

To arrive at a condition for solving $c_0(\zeta)$ we look to $O(\delta^2)$, which is a partial differential equation for $c_2(r,\zeta,t)$:

$$\alpha^2 Sc \frac{\partial c_2}{\partial t} - \frac{\partial^2 c_2}{\partial r^2} - \frac{1}{r}\frac{\partial c_2}{\partial r} = \frac{\mathrm{d}^2 c_0}{\mathrm{d}\zeta^2} - Sc\left[w_1 \frac{\mathrm{d}c_0}{\mathrm{d}\zeta} + w_0 \frac{\partial c_1}{\partial \zeta} + u_0 \frac{\partial c_1}{\partial r}\right], \tag{6.5}$$

with the corresponding no-flux condition

$$\frac{\partial c_2(1,\zeta,t)}{\partial r} = -\eta_1 \frac{\partial^2 c_1(1,\zeta,t)}{\partial r^2}. \tag{6.6}$$

Note that in the above equation, the unsteady term is balanced by terms

representing radial convection and axial diffusion as well as radial diffusion and axial convection; also, the no-flux condition is non-homogeneous and contains the wall position explicitly. The products of the unsteady velocities and concentration gradients on the right-hand side of (6.5) generate both steady and unsteady quantities, so that the $O(\delta^2)$ equation has a solution of the form

$$c_2 = C_2^{(s)}(r,\zeta) + C_2^{(1)}(r)\,\mathrm{e}^{-\mathrm{i}(k\zeta - t)} + C_2^{(2)}(r)\,\mathrm{e}^{-2\mathrm{i}(k\zeta - t)} + \text{c.c.} \tag{6.7}$$

The differential equation for the steady component of c_2 provides the necessary condition to determine $c_0(\zeta)$. Integrating this equation over the cross-section gives

$$r\frac{\mathrm{d}c_2^{(s)}}{\mathrm{d}r}\bigg|_{r=0}^{r=1} = -\frac{\mathrm{d}^2 c_0}{2\mathrm{d}\zeta^2} + Sc\int_0^1 \left[\left(u_0\frac{\partial c_1}{\partial r}\right)^{(s)} + \left(w_0\frac{\partial c_1}{\partial \zeta}\right)^{(s)} + w_1^{(s)}\frac{\mathrm{d}c_0}{\mathrm{d}\zeta}\right]\mathrm{d}r, \tag{6.8}$$

where the superscript (s) denotes the steady component of each quantity. Next, the chain rule is applied to the third term on the right-hand side above, the second term on the right-hand side is integrated by parts, and the conservation of fluid mass condition (equation (2.4)) is implemented. Applying the no-flux condition and substituting the results obtained earlier for the velocity components and concentration, we obtain a second-order ordinary differential equation for $c_0(\zeta)$:

$$\frac{\mathrm{d}^2 c_0}{\mathrm{d}\zeta^2}[1 - a_1\,\mathrm{e}^{2k_{\mathrm{I}}\zeta}] + a_2\,\mathrm{e}^{2k_{\mathrm{I}}\zeta}\frac{\mathrm{d}c_0}{\mathrm{d}\zeta} = 0. \tag{6.9}$$

Integrating this equation twice and implementing the end conditions gives

$$c_0(\zeta) = -\frac{\displaystyle\int_0^\zeta F(s)\,\mathrm{d}s}{\displaystyle\int_0^l F(s)\,\mathrm{d}s} + 1, \tag{6.10}$$

where the function $F(s)$ is given by

$$F(s) = [1 - a_1\,\mathrm{e}^{2k_{0\mathrm{I}}s}]^{a_2/(2k_{0\mathrm{I}})\,a_1}, \tag{6.11}$$

and

$$a_1 = 2Sc\int_0^1 \overline{W}_0\,C_1\,r\,\mathrm{d}r, \tag{6.12a}$$

$$a_2 = -2\left\{\bar{H}_0\frac{\partial^2 C_1^{(1)}}{\partial r^2} + Sc\left[\bar{U}_1^{(1)}C_1^{(1)} + \int_0^1 [W_1^{(0)} + 2k_{0\mathrm{I}}\,\overline{W}_0\,C_1]\,r\,\mathrm{d}r\right]\right\}. \tag{6.12b}$$

Note that the expression for $c_1(r,\zeta,t)$ is now complete since $\mathrm{d}c_0/\mathrm{d}\zeta$ can be calculated from (6.10).

As the flexible tube under consideration becomes very stiff, it can be shown that the wavenumber, k, and the constant a_2 approach zero, so that the above expression for $c_0(\zeta)$ becomes linear in ζ. This is consistent with long-wave theory, since the rigid-tube result is obtained in the limit $\kappa \to \infty$.

7. Concentration field: results

Assigning the same values to the dimensionless parameters as discussed earlier, and with $Sc = 0.882$, the effect of wall flexibility on the concentration field over a range of frequencies is examined. In the rigid tube, the axial concentration gradient is a constant, so that $c^{(s)}$ is a linear function of ζ for all values of α. The corresponding $c^{(s)}$ in the flexible-tube problem is the leading-order concentration, c_0; in our analysis,

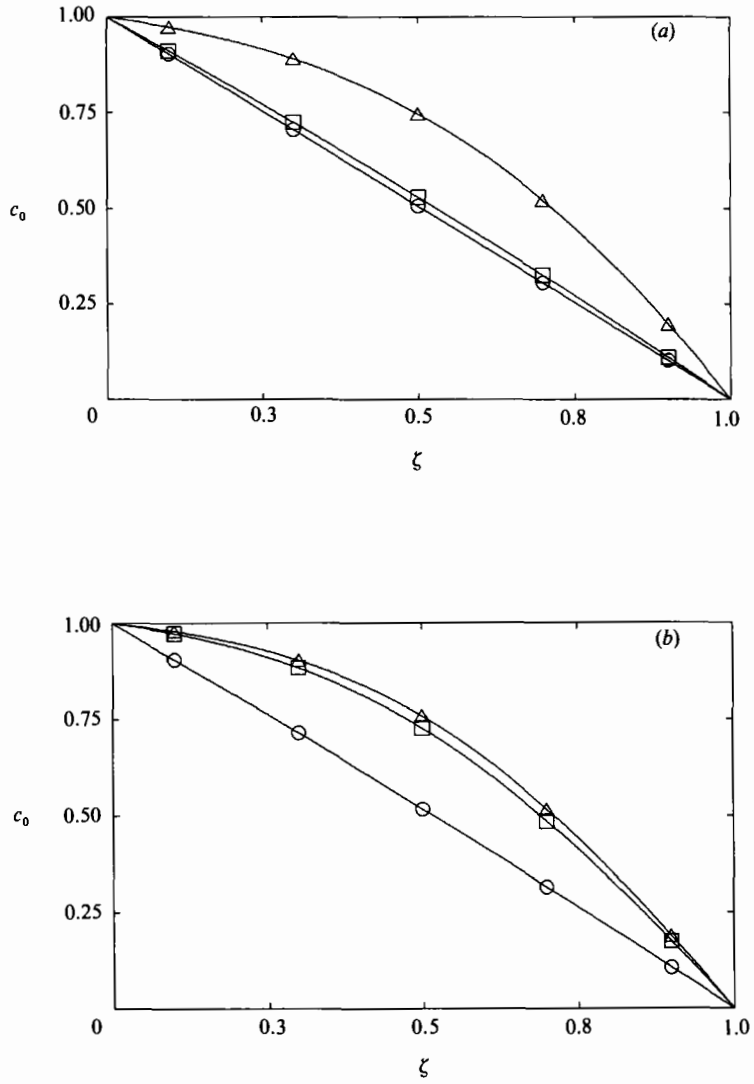

FIGURE 3. Steady concentration profile as a function of ζ, for ○, $\alpha = 2$; □, $\alpha = 6$; △, $\alpha = 10$; (*a*) $\kappa = 10^4$; (*b*) $\kappa = 10^3$.

$\kappa = 10^8$ gives the expected linear concentration profile. However, as κ decreases, the dependence of c_0 on ζ becomes nonlinear and frequency dependent. Figure 3(*a*, *b*) illustrates c_0 as a function of ζ for $\alpha = 2$, 6, and 10 for the two cases $\kappa = 10^4$ and $\kappa = 10^3$. For $\alpha = 2$, both values of κ give nearly linear concentration profiles. However, as frequency increases to $\alpha = 6$ and $\alpha = 10$, the profiles become nonlinear as they curve upward.

8. Mass transport

The objective of this analysis is to determine the time-mean longitudinal transport of the species through the flexible tube under conditions of volume-cycled flow with uniform steady end concentrations. This quantity, the steady rate of axial mass transport, can be expressed by the integral of the convective and diffusive transport

across the cross-section, averaged over one period. In dimensionless form, this steady axial mass transport rate is given by

$$m = \frac{1}{2\pi}\int_{t_0}^{t_0+2\pi}\int_0^{2\pi}\int_0^{1+\eta}\left[wc - \frac{1}{Sc}\delta\frac{\partial c}{\partial \zeta}\right] r\,\mathrm{d}r\,\mathrm{d}\theta\,\mathrm{d}t. \tag{8.1}$$

In the above expression, the dimensional steady transport rate, which has units of mass per unit time, has been scaled so that $m = m^*/(a\nu\hat{c})$.

We can insert the asymptotic expansions found as solutions for w and c into the above equation, noting that the time-periodic terms integrate to zero, to obtain an expansion for the steady rate of transport:

$$m = 2\pi\delta\int_0^1 \left\{e^{2k_1\zeta}[\overline{W}_0 C_1 + W_1^{(0)}c_0 + \text{c.c.}] - \frac{1}{Sc}\frac{\partial c_0}{\partial \zeta}\right\} r\,\mathrm{d}r + O(\delta^2). \tag{8.2}$$

It may appear that the above expression for axial transport depends on the axial coordinate ζ. However, in order for mass to be conserved, the steady transport of contaminant through any cross-section must be constant, so that m is actually independent of ζ.

9. Mass transport: results

Assigning the same values to the dimensionless parameters as discussed earlier, the effect of wall flexibility on the steady mass transport rate over a range of frequencies is examined.

Fig. 4 illustrates the relationship between m and α for $\kappa = 10^3$, 10^4, 10^5, and 10^8. Here we are able to see the effect of wall flexibility on the rate of mass transport. The curve corresponding to $\kappa = 10^8$ coincides with mean mass transport in a rigid tube. For smaller κ, the mass transport is less than or equal to that of the rigid tube for all α; in fact, as κ decreases, m also decreases for most α in the parameter range considered. Experimental observations appear to be in agreement with the trend of the results presented here: a decrease in gas exchange efficiency due to radial airway motion was observed by Gavriely *et al.* (1985) in cineradiobronchograms of dog lungs undergoing high-frequency ventilation. Because air is shunted in the radial direction by the wall motion, axial transport of a diffusible species is reduced. Likewise, our theory indicates that lower wall stiffness (lower κ) leads to increased wall motion (figure 1*a*) and to reduced mass transport rates. The mechanism, however, is more complicated as we now explore.

Another important aspect of figure 4 is the presence of a local maximum on the $\kappa = 10^4$ and $\kappa = 10^3$ curves. A maximum m for the $\kappa = 10^5$ curve may exist outside the parameter range; however, for rigid tubes m increases monotonically with α. The presence of a local maximum mass transport rate is significant, since it suggests that an optimal oscillation frequency exists. We also note that the frequency at which m reaches its peak is dependent on κ. Very flexible tubes appear to give the best transport at low α, and stiffer tubes reach their maximum transport rate at higher α. Note the similarity between the m versus α curves, figure 4, and the ϕ versus α curves, figure 1 (*b*). These two figures appear to be inverses of each other; not only are their shapes similar, but the maximum mass transport rate on each curve occurs at a value of α near the minimum phase angle. This observation suggests that the delay between the volume flow rate and the response of the tube wall is a significant factor in determining the rate of mass transport. The highest transport rate for any given κ appears to occur roughly when the wall response is closest to being in phase

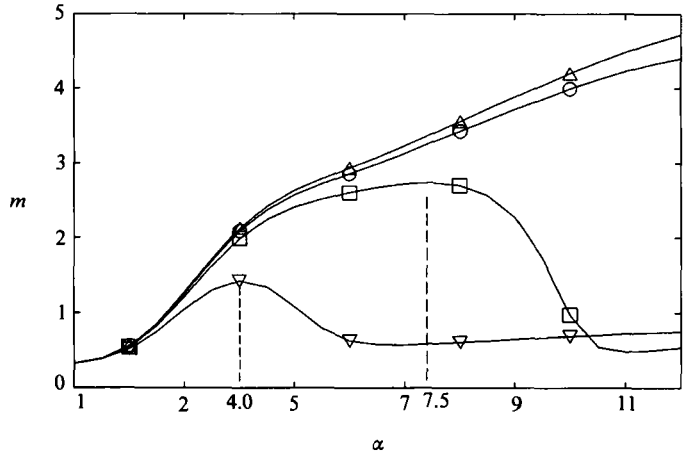

FIGURE 4. Steady mass transport rate as a function of α, for ∇, $\kappa = 10^3$; $\square$, $\kappa = 10^4$; $\bigcirc$, $\kappa = 10^5$; $\triangle$, $\kappa = 10^8$.

with the flow. When no minimum phase difference occurs, as in the case $\kappa = 10^8$, no maximum value of m occurs. Also, the α values for maximal mass flow rate are far from those for maximal amplitude, D, in figure 1 (a), suggesting that the magnitude of lateral shunting may not be as important as how it affects the phase relationship between flow and wall motion.

Up to this point in the analysis, the amplitude parameter A has been held fixed at $A = 5$. In high-frequency ventilation, the rate of gas exchange (or mass transport) as a function of tidal volume ($V_T = A(\pi a^3)$) is of interest, so the effect of changing A is shown in figure 5 (a–c). For rigid tubes we know that m is proportional to A^2 independent of α, a slope of 2 in these log–log plots. In figure 5 (a), where $\alpha = 2$, m is plotted against A for various values of κ. Clearly the slopes here are less than 2. In figure 5 (b), $\alpha = 6$, and the slope of 2 is apparent in the stiffer tubes for $A > 3$, approximately, but the $\kappa = 10^3$ tube shows a slope of approximately 0.9 or less. Figure 5 (c) shows, for $\alpha = 10$, the drop off in slope for both the $\kappa = 10^3$ and 10^4 tubes. All three figures show that the axial mass transport increases with increasing stroke amplitude.

Examining each term in the expression for m given by (8.2), we find that the diffusion and steady drift terms are unaffected by changes in ϕ, and that the convective term is responsible for the behaviour of the low-κ curves in figure 4. It is the integral of the product $(rw_0 c_1)^{(s)}$ that is responsible for the existence of a maximum rate of transport. We examine the distribution of $(rw_0 c_1)^{(s)}$ over the cross-section of the tube at $\zeta = 0$ for several values of α and $\kappa = 10^4$ (figure 6a), and $\kappa = 10^8$ (figure 6b). In both cases it is interesting to note that the contribution to m is negative near the tube wall and, for $\alpha > 6$, in the centre of the tube. The positive contribution to m comes from the interaction of w_0 and c_1 in the middle region of the profile. In the nearly rigid-tube case (figure 6b), the peak value of the convective term increases as α increases. However, in the more flexible tube (figure 6a), the peak value of the convective term increases with α when α is small, but decreases with α for $\alpha > 8$. Thus, as the frequency of oscillation increases in low-κ tubes, the interaction of w_0 and c_1 is inhibited so that mass transport is reduced.

As discussed earlier, convection and diffusion interact during oscillatory flow to enhance the axial mass transport rate over that which would occur by diffusion alone. Often, this enhancement is expressed as an effective diffusivity, D^*_{eff}, defined

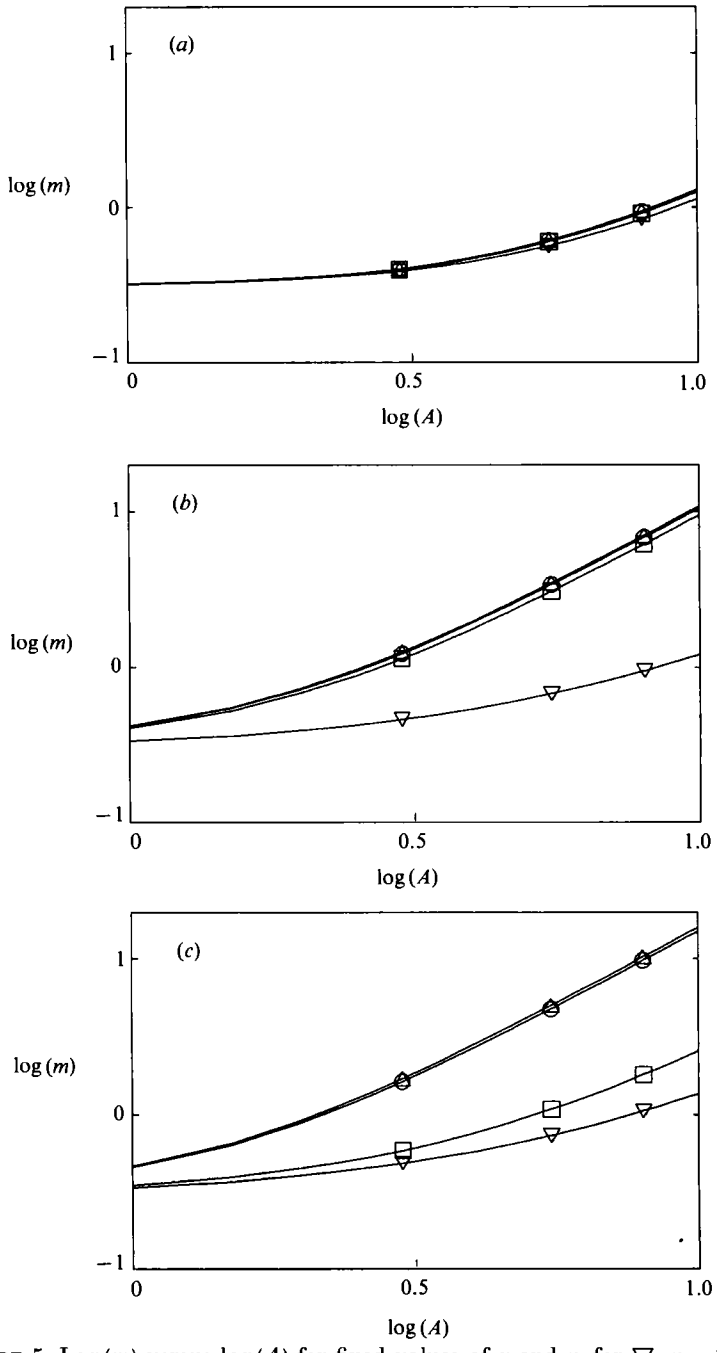

FIGURE 5. Log (m) versus log (A) for fixed values of α and κ, for $\triangledown$, $\kappa = 10^3$; $\square$, $\kappa = 10^4$; $\bigcirc$, $\kappa = 10^5$; $\triangle$, $\kappa = 10^8$ for (a) $\alpha = 2$, (b) $\alpha = 6$, (c) $\alpha = 10$.

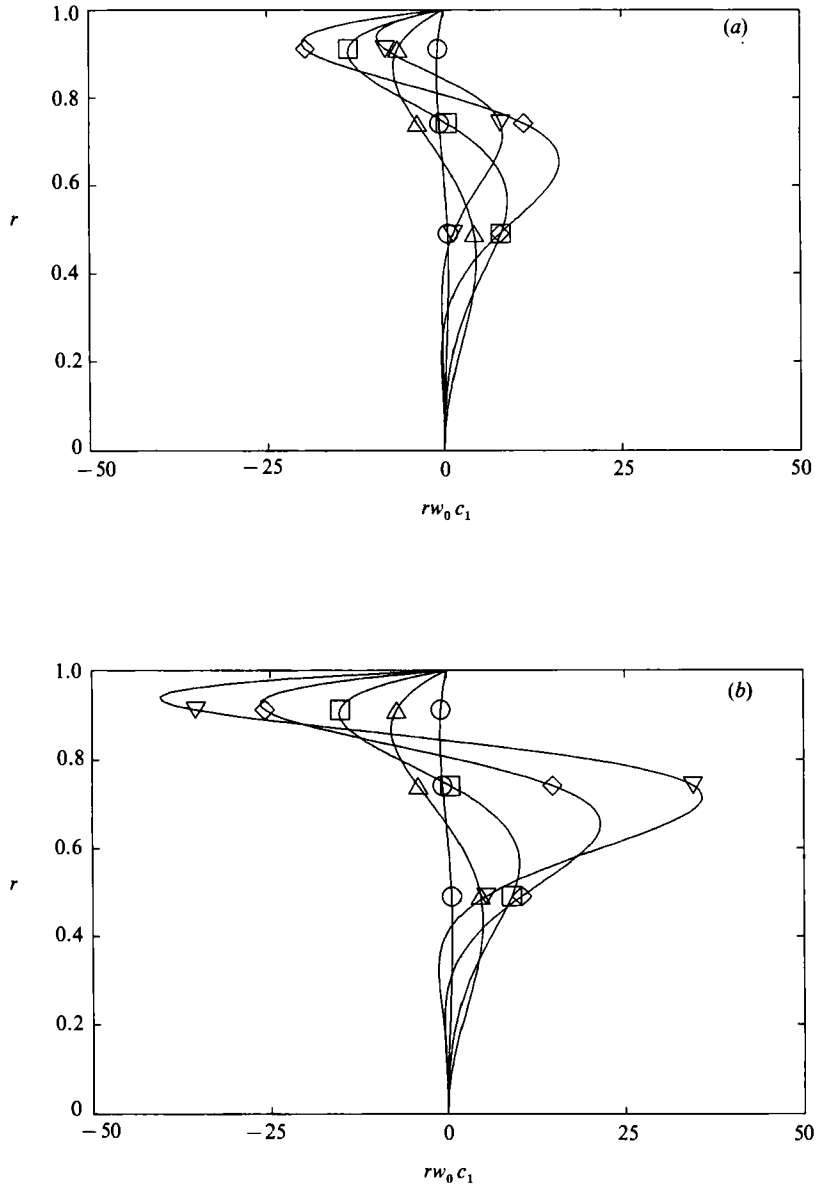

FIGURE 6. Steady product of $w_0(r)$, $c_1(r)$, and r at $\zeta = 0$ as a function of r, for ○, $\alpha = 2$; △, $\alpha = 4$; □, $\alpha = 6$; ◇, $\alpha = 8$; ▽, $\alpha = 10$: (*a*) $\kappa = 10^4$; (*b*) $\kappa = 10^6$.

as the ratio of the time-averaged mass flux to the steady axial concentration gradient. Scaling D^*_{eff} on the molecular diffusivity, so that $D_{\text{eff}} = D^*_{\text{eff}}/D_{\text{m}}$, the dimensionless effective diffusivity can be expressed as

$$D_{\text{eff}} = \frac{-mSc}{\pi\delta\, \mathrm{d}c_0/\mathrm{d}\zeta}. \tag{9.1}$$

In rigid tubes, the axial concentration gradient is constant, so that D_{eff} differs from the mass transport rate, m, by a constant. However, in the flexible-tube analysis presented here, the relationship between m and D_{eff} is not as simple; m is independent

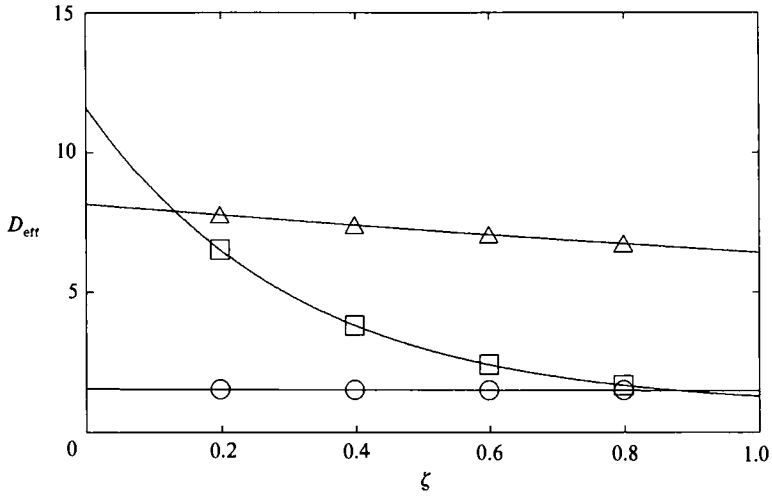

FIGURE 7. Time-averaged effective diffusivity as a function of ζ, for $\kappa = 10^4$ and ○, $\alpha = 2$; △, $\alpha = 6$; □, $\alpha = 10$.

of z while D_{eff} is not, since dc_0/dz is not a constant. Figure 7 illustrates how D_{eff} decreases along the ζ-axis for $\alpha = 2$, 6, and 10 and $\kappa = 10^4$. Note that the rate of decay is larger when the frequency α is higher. Although the $\alpha = 10$ curve has a higher effective diffusivity near $\zeta = 0$, its rapid decay results in a lower effective diffusivity than the $\alpha = 6$ curve over most of the length of the tube; as a result, axial mass transport is better when $\alpha = 6$ than when $\alpha = 10$, as illustrated earlier in figure 4. Perhaps a more useful descriptor is to characterize the tube's transport ability by using its fixed, time-averaged concentration difference at the $\zeta = 0$ and $\zeta = 1$ axial positions. If we call G_{ax} the axial conductance and define it as the ratio of mass flux, $(m^*/\pi a^2)$, to the overall concentration gradient, $\Delta C^*/\Delta z^*$, we arrive at the relationship

$$G_{\text{ax}} = \frac{mSc}{\pi}\frac{L}{a}. \tag{9.2}$$

Then G_{ax} is related to the graphs of m in figures 4 and 5 by the above multiple, where L is the axial length over which the concentration gradient is fixed. For our example, $L/a = 10$.

10. Discussion

Transport in flexible tubes is enhanced by volume-cycling of the fluid over that of pure diffusion, at least over a range of frequencies. This can be attributed to the interaction of axial convection with radial diffusion; solute diffuses radially to regions of higher axial velocity. Our results indicate that the enhancement of transport in flexible tubes is less than that in rigid tubes. Also, tube flexibility introduces the presence of a maximum transport rate, which occurs when the motion of the tube wall in response to the volume cycling is most in phase with the volume flow rate.

In this study we have chosen parameter values that are relevant to gas transport in the pulmonary airways. If we apply the results above to ventilation, we can think of fixed A as constant tidal volume and increasing α as increasing breathing frequency. The presence of the local maximum in the m versus α curves may explain,

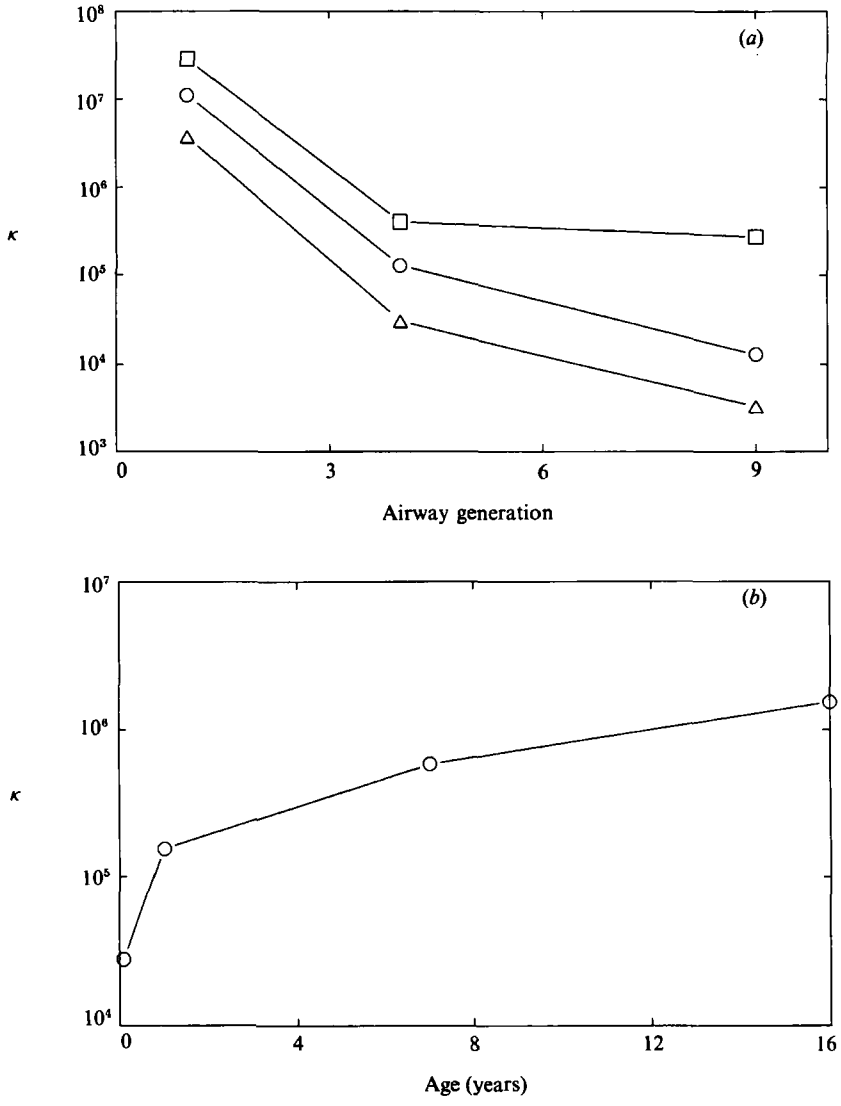

FIGURE 8. (*a*) κ as a function of airway generation in excised dog lungs. Curves shown are for transmural pressures in the range: △, 0–5 cm saline; ○, 10–15 cm saline; □, 20–25 cm saline; (*b*) κ of the human trachea as a function of age. Transmural pressure = 5 cm water.

in part, the experimental results of Slutsky *et al.* (1980), Rieke *et al.* (1983), Mitzner *et al.* (1983), and Rossing *et al.* (1981), in which gas exchange efficiency peaked or plateaued with increasing frequency of oscillation. In a clinical setting it is important to know whether to attribute such behaviour to pathology or to the complex mass transport characteristics of a normal lung.

Another point to note is that the maximum transport rate depends on κ, suggesting the existence of an optimal frequency of oscillation during HFV that depends on lung compliance. Stiffer airways (high κ) would more effectively be ventilated at a higher frequency than softer airways (low κ). We also note the possibility of using these characteristics as a diagnostic tool; a diseased lung may be characterized by a measured gas exchange efficiency that peaks at a particularly high or low frequency. It is essential to consider how κ varies with airway generation;

locating low-κ generations may enable us to identify the airways that are responsible for limiting gas transport. Martin & Proctor (1958) made pressure–volume measurements on three different sizes of excised dog bronchi that roughly correspond to the first, fourth, and ninth airway generations. Based on their data, κ can be plotted as a function of airway generation for several transmural pressure intervals, as shown in figure 8(*a*).The plot illustrates that deeper airways tend to have the lowest κ, so they may become important limiters of transport. Also, at higher transmural pressure intervals κ is larger in all airways, suggesting that HFV might be more effective when a steady pressure, such as positive end expiratory pressure (PEEP) is superimposed over the oscillatory one. Age also plays a role in determining a patient's optimal breathing frequency. Pressure–volume measurements from Croteau & Cook (1961), along with the assumption that tracheal radii vary linearly with size, can be used to calculate κ in the trachea for humans ranging in age from newborn infants to sixteen year olds, as illustrated in figure 8(*b*).

Several investigations of high-frequency ventilation in animals and hardware models regress the collected mass transport data as a product of frequency and tidal volume (Paloski, Slosberg & Kamm 1987; Tarbell, Ultman & Durlofsky 1982; Rossing *et al.* 1981). In our notation such a relationship would appear as $m \approx \alpha^b A^e$, where b and e are empirical constants. In a straight, rigid tube $e = 2$, while $b = 4$ for small α and $b = 1$ for large α. As a counter-example, however, figure 4 shows that $b < 1$ for large α in stiffer tubes and $b < 0$ for large α in the softer tubes. Also, figure 5 shows that e is α-dependent when flexibility is important. Such simple regressions, therefore, may not be readily transferred from rigid branching network models to intact animals when airway compliance is significant.

This work was supported by NIH grants HL-01818, HL-41126 and HL-35440.

Appendix. Dimensional values

In computing the results for the velocity field, wave characteristics, etc. we are interested in the effect of wall flexibility over a range of frequencies. Therefore, the other parameters of the problem are fixed. In choosing constants for the problem, effort was made to choose constants that are relevant to gas transport in the trachea. The dimensional parameters have the following values:

inner radius of undeformed tube (trachea):	$a = 0.9$ cm
tube thickness:	$h = 0.05$ cm
kinematic viscosity (of air):	$\nu = 0.15$ cm^2/s
molecular diffusivity (of CO_2 in air):	$D_m = 0.17$ cm^2/s
fluid density (air):	$\rho = 0.001\,14$ g/cm^3
wall density:	$\rho_0 = 0.997$ g/cm^3
Poisson's ratio:	$\gamma = 0.5$
tube length:	$l = 10$ cm
wall damping:	$g = 5.0$ s^{-1}
Tidal volume (for $A = 5$)	$V_T = 11.5$ cm^3
frequency (for $1 \leqslant \alpha \leqslant 12$)	$0.03 \leqslant f \leqslant 4.3$
modulus of elasticity (for $10^3 \leqslant \kappa \leqslant 10^8$)	$28 \leqslant E \leqslant 2.8 \times 10^6$ g/(cm s^2)

REFERENCES

ATABEK, H. B. & LEW, H. S. 1966 Wave propagation through a viscous incompressible fluid contained in an initially stressed elastic tube. *Biophys. J.* **6**, 481–503.

BOHN, D. J., MIYASAKA, K., MARCHAK, E. B., THOMPSON, W. K., FROESE, A. B. & BRYAN, A. C. 1980 Ventilation by high-frequency oscillation. *J. Appl. Physiol.* **48**, 710–716.

CHATWIN, P. C. 1975 On the longitudinal dispersion of passive contaminant in oscillatory flows in tubes. *J. Fluid Mech.* **71**, 513–527.

CROTEAU, J. R. & COOK, C. D. 1961 Volume-pressure and length-tension measurements in human tracheal and bronchial segments. *J. Appl. Physiol.* **16**, 170–172.

ECKMAN, D. M. & GROTBERG, J. B. 1988 Oscillatory flow and mass transport in a curved tube. *J. Fluid Mech.* **188**, 509–527.

GAVER, D. P. & GROTBERG, J. B. 1986 An experimental investigation of oscillating flow in a tapered channel. *J. Fluid Mech.* **172**, 47–61.

GAVRIELY, N., SHEE, T. R., CUGELL, D. W. & GROTBERG, J. B. 1989 Flutter in flow-limited collapsible tubes: a mechanism for generation of wheezes. *J. Appl. Physiol.* **66**, 2251–2261.

GAVRIELY, N., SOLWAY, J., DRAZEN, J. M., SLUTSKY, A. S., BROWN, R., LORING, S. H. & INGRAM, R. H. 1985 Radiographic visualization of airway wall movement during oscillatory flow in dogs. *J. Appl. Physiol.* **58**, 645–652.

GODLESKI, D. A. & GROTBERG, J. B. 1988 Convection-diffusion interaction for oscillatory flow in a tapered tube. *J. Biomech. Engng* **110**, 283–291.

GROTBERG, J. B. 1984 Volume-cycled oscillatory flow in a tapered channel. *J. Fluid Mech.* **141**, 249–264.

HARRIS, H. G. & GOREN, S. L. 1967 Axial diffusion in a cylinder with pulsed flow. *Chem. Engng Sci.* **22**, 1571–1576.

JOSHI, C. H., KAMM, R. D., DRAZEN, J. M. & SLUTSKY, A. S. 1983 An experimental study of gas exchange in laminar oscillatory flow. *J. Fluid Mech.* **133**, 245–254.

MARTIN, H. B. & PROCTOR, D. F. 1958 Pressure-volume measurements on dog bronchi. *J. Appl. Physiol.* **13**, 337–343.

MITZNER, W., PERMUTT, S. & WIENMANN, G. 1983 A model of airway gas transport during high frequency ventilation. *Ann. Biomed. Engng* **11**, 61.

PALOSKI, W. H., SLOSBERG, R. B. & KAMM, R. D. 1987 Effects of gas properties and waveform asymmetry on gas transport in a branching tube network. *J. Appl. Physiol.* **62**, 892–901.

PEDLEY, T. J. & KAMM, R. D. 1988 The effect of secondary motion on axial transport in oscillatory tube flow. *J. Fluid Mech.* **193**, 347–367.

RIEKE, H., HOOK, C. & MEYER, M. 1983 Pulmonary gas exchange during high frequency ventilation in dogs. *Respir. Physiol.* **54**, 1–17.

ROSSING, T. H., SLUTSKY, A. S., LEHR, J. L., DRINKER, P. A., KAMM, R. D. & DRAZEN, J. M. 1981 Tidal volume and frequency dependence of carbon dioxide elimination by high frequency ventilation. *New Engl. J. Med.* **305**, 1375–1379.

SHARP, M. K., KAMM, R. D., SHAPIRO, A. H., KIMMEL, E. & KARNIADAKIS, G. E. 1991 Dispersion in a curved tube during oscillatory flow. *J. Fluid Mech.* **223**, 537–563.

SIMON, B. A., WEINMANN, G. G. & MITZNER, W. 1984 Mean airway pressure and alveolar pressure during high-frequency ventilation. *J. Appl. Physiol.* **57**, 1069–1078.

SLUTSKY, A. S., DRAZEN, J. M., INGRAM, R. H., KAMM, R. D., SHAPIRO, A. H., FREDBERG, J. J., LORING, S. H. & LEHR, J. 1980 Effective pulmonary ventilation with small-volume oscillations at high frequency. *Science* **209**, 609–611.

TARBELL, J. M., ULTMAN, J. S. & DURLOFSKY, L. 1982 Oscillatory dispersion in a branching tube network. *J. Biomech. Engng* **104**, 338–342.

WATSON, E. J. 1983 Diffusion in oscillatory pipe flow. *J. Fluid Mech.* **133**, 233–244.